

1 **A New Probabilistic Wave Breaking Model for**
2 **Dominant Wind-sea Waves Based on the Gaussian**
3 **Field Theory**

4 **C. E. Stringari¹, M. Prevosto², J.-F. Filipot¹, F. Leckler¹, P. V. Guimarães^{1,3}**

5 ¹France Energies Marines, Plouzané, France

6 ²Institut Français de Recherche pour l'Exploitation de la Mer, Plouzané, France

7 ³PPGOceano, Federal University of Santa Catarina, Florianópolis, 88040-900, Brazil

8 **Key Points:**

- 9 • A new probabilistic wave breaking model based on Gaussian field theory is pre-
10 sented for dominant, wind-sea waves.
- 11 • Wave breaking probabilities are modeled from the joint probability density between
12 wave phase speed and particle orbital velocity.
- 13 • The proposed model performs well when compared to six other historical mod-
14 els using three field datasets.

Corresponding author: C.E. Stringari, Caio.Stringari@france-energies-marines.org

Corresponding author: J.F. Filipot, Jean.Francois.Filipot@france-energies-marines.org

15 Abstract

16 This paper presents a novel method for obtaining the probability wave of break-
17 ing (P_b) of deep water, dominant wind-sea waves (that is, waves made of the energy within
18 $\pm 30\%$ of the peak wave frequency) derived from Gaussian wave field theory. For a given
19 input wave spectrum we demonstrate how it is possible to derive a joint probability den-
20 sity function between wave phase speed (c) and horizontal orbital velocity at wave crest
21 (u) from which a model for P_b can be obtained. A non-linear kinematic wave breaking
22 criterion consistent with the Gaussian framework is further proposed. Our model would
23 allow, therefore, for application of the classical wave breaking criterion (that is, wave break-
24 ing occurs if $u/c > 1$) in spectral wave models which, to the authors' knowledge, has not
25 been done to date. Our results show that the proposed theoretical model has errors in
26 the same order of magnitude as six other historical models when assessed using three field
27 datasets. With optimization of the proposed model's single free parameter, it can be-
28 come the best performing model for specific datasets. Although our results are promis-
29 ing, additional, more complete wave breaking datasets collected in the field are needed
30 to comprehensively assess the present model, especially in regards to the dependence on
31 phenomena such as direct wind forcing, long wave modulation and wave directionality.

32 Plain Language Summary

33 Waves will break if the speed of the water particles on the wave crest is greater than
34 the speed of the wave itself, causing the wave crest to overtake the front part of the wave,
35 leading to wave breaking. Precisely simulating real ocean waves requires, therefore, a particle-
36 by-particle description of the water motion, which is too expensive for the current com-
37 puters to handle in real-world applications. Instead, wave models describe waves by means
38 of their statistical properties, that is, averaged over a large number of waves. In this pa-
39 per, we present a mathematical formulation that allows to calculate the combined prob-
40 ability between the speed of particles on the wave crest and the wave speed based only
41 on statistical properties. From these combined probabilities, we model the probability
42 of wave breaking. Our results indicate that our model performed relatively well when
43 compared to six other models using three historical datasets. Because of a lack of ob-
44 served data to assess our model, we recommend that future research should focus on col-
45 lecting more wave breaking data measured in the field. Future advances on this line of

46 research could lead, for example, to improvements on operational weather forecast mod-
47 els.

48 **1 Introduction**

49 A robust description of wave breaking is a crucial aspect of wave modelling. It is
50 via wave breaking that most of the wave energy is dissipated and a precise formulation
51 of this phenomenon is required to obtain reliable models. Despite of its importance, en-
52 ergy dissipation due to wave breaking is still modelled as a semi-empirical process due
53 to the difficulty to represent physically-derived wave breaking criteria on phase-averaged
54 wave models (Battjes & Janssen, 1978; Thornton & Guza, 1983; Banner et al., 2000; Fil-
55 ipot et al., 2010; Filipot & Ardhuin, 2012; Banner et al., 2002; Ardhuin et al., 2010; Ban-
56 ner et al., 2014; Zieger et al., 2015; Ardag & Resio, 2020). The available probabilistic
57 (that is, parametric, or empirical) formulations included in these models have been de-
58 rived from limited datasets and without rigorous theoretical frameworks and, therefore,
59 they currently lack a solid physical background. While the current operational (spectral)
60 models are capable of reproducing field observations of integrated spectral parameters
61 (for example, significant wave height, peak wave period and peak wave direction) with
62 good accuracy, it remains unclear if their wave breaking parameterizations are entirely
63 reliable. This knowledge gap partly occurs because limited research has focused on wave
64 breaking statistics derived from field data, especially when it comes to wave breaking ob-
65 servations distributed as a function of wave scales (for example, wave frequency or wave
66 phase speed). The research developed here has, therefore, important implications for air-
67 sea flux parameterizations (Kudryavtsev et al., 2014), safety at sea (Kjeldsen et al., 1980)
68 and design of offshore structures (Filipot et al., 2019), all of which directly rely on the
69 properties of breaking waves.

70 Historically, parametric wave breaking models have been constructed from two dif-
71 ferent approaches: the first approach considers wave statistics (wave steepness, most fre-
72 quently) derived from a wave-by-wave analysis of the surface elevation timeseries collected
73 at a single point location where wave breaking occurrences are synchronously identified
74 (using video data, most frequently). The wave breaking probability (that is, the ratio
75 between the total number of breaking waves over the total number of waves during a given
76 period of time) can then be expressed as a bulk quantity (Thornton & Guza, 1983; Chawla
77 & Kirby, 2002; Alsina & Baldock, 2007; Janssen & Battjes, 2007) or can be distributed

78 over wave frequency (f), wavenumber (k), or wave speed (c) ranges, referred as to “wave
79 scales” by the wave modelling community (Eldeberky & Battjes, 1996; Banner et al., 2002;
80 Filipot et al., 2010).

81 The second approach follows from Phillips (1985) who defined the distribution $\Lambda(c)dc$
82 as the “average total length per unit surface area of breaking fronts that have velocities
83 in the range c to $c+dc$ ”. This approach therefore relates to the analysis of sea surface
84 images in which individual wave breaking patches are tracked in space and time. The
85 main motivation for introducing this new concept was clearly stated in Phillips (1985):
86 “There is clearly some association of the breaking events with waves of different scales,
87 but it is difficult to make the association in an unambiguous way if we consider only the
88 surface configuration at one given instant. A breaking crest may indeed be a local max-
89 imum in the instantaneous surface configuration but there is no guarantee that a local
90 wavelength of the breaking wave can be defined clearly. It seems more satisfactory to
91 use the velocity c of the breaking front as a measure of the scale of the breaking”. This
92 quotation clearly identify the limitations of directly relying on the analysis of single point
93 elevation timeseries. Different parameterizations have been proposed to quantity $\Lambda(c)dc$
94 from theoretical (Phillips, 1985) or empirical considerations (Melville & Matusov, 2002;
95 Sutherland & Melville, 2013; Romero, 2019). However, Phillips’ (1985) framework re-
96 mains controversial, particularly regarding its practical application, given that different
97 interpretations of his concepts can generate differences of several orders of magnitude
98 in the calculations of $\Lambda(c)dc$ and its moments (Banner et al., 2014). For a detailed re-
99 view of commonly used parametric wave breaking models please refer to Appendix A.

100 Interestingly, while the ratio between the horizontal orbital velocity at the crest (u)
101 to wave phase speed (c) appears the most reliable parameter to determine wave break-
102 ing occurrence (Saket et al., 2017; Barthelemy et al., 2018; Derakhti et al., 2020; Var-
103 ing et al., 2020), it was not used by any of the approaches mentioned above. This pa-
104 per provides a new promising wave breaking model by revisiting Rice (1944) and Longuet-
105 Higgins (1957) statistical descriptions of Gaussian processes (that is, for linear waves)
106 to obtain the theoretical joint probability density between c and u ($p(c, u)$). We then
107 model P_b assuming a kinematic wave breaking criterion consistent with non-linear waves,
108 that is, a wave breaks if the fluid velocity at the wave crest is greater than the wave phase
109 speed ($u > c$). This study focuses on analysing dominant waves, defined as waves that
110 have frequencies within $\pm 30\%$ of the spectral peak frequency of the wind-sea (Banner

111 et al., 2000). Future research will be dedicated to extend our efforts to broader wave scales.
 112 This paper is organized as follows: Section 2 describes the proposed model, Section 3 presents
 113 three historical datasets used to evaluate the model, Section 4 presents the results, Sec-
 114 tion 5 discusses and Section 6 concludes.

115 **2 Definition of a Probabilistic Wave Breaking Model Based on Gaus-**
 116 **sian Field Theory**

117 The kinematic wave breaking criterion $u/c = 1$ has been historically used as the
 118 onset of wave breaking for non-linear, real waves (see Perlin et al. (2013) for a review).
 119 Recently, Barthelemy et al. (2018) found and Derakhti et al. (2020) confirmed via nu-
 120 merical simulations that waves will inevitably start to break shortly after u/c exceeds
 121 0.85 in deep and shallow water. Further numerical simulations showed that wave break-
 122 ing occurs when the maximum orbital velocity (u_{max}) equals c somewhere along the wave
 123 profile and not necessarily at the wave crest (Varing et al., 2020). Although the relation-
 124 ship u/c provides a solid physical background to establish the onset of wave breaking,
 125 this approach has never been applied to spectral wave models because it requires phase-
 126 resolving the wave field. In the sections below, we circumvent this difficulty by defining
 127 a wave breaking probability model using the joint probability density between c and u
 128 corresponding to a given wave energy spectrum ($E(f)$). The efforts in this paper are con-
 129 sistent with part of the recent work from Ardag and Resio (2020) in the sense that both
 130 works aim to solidify the use of the kinematic wave breaking criterion as the standard
 131 approach for modelling wave breaking.

132 **2.1 Theoretical Derivation of the Joint Probability Density Distribu-**
 133 **tion of Orbital Velocity at the Wave Crest and Phase Speed**

134 Longuet-Higgins (1957) published a very complete work on the statistics of Gaus-
 135 sian wave fields. In particular, Longuet-Higgins (1957) studied the probability density
 136 of the speed of zero-crossings along a given line that is of interest for us in this work. In
 137 his paper, the speed of zero-crossings were applied in particular to the zero-crossings of
 138 the space derivative of a Gaussian process, that is, the velocities of the local maxima in
 139 space (Longuet-Higgins (1957), pp. 356-357). The present work describes how the same
 140 methodology can be extended to derive the joint density of the speed of space local max-
 141 ima (or local crests) and simultaneous wave horizontal orbital velocity for a one-dimensional

142 Gaussian sea state. For simplicity, this paper follows the same notations as those of Longuet-
 143 Higgins (1957) and the reader is directed to Section 2.5 in Longuet-Higgins (1957) for
 144 further details.

145 As explained in Longuet-Higgins (1957), if $\xi_1(x, t)$ is a stationary-homogeneous pro-
 146 cess and we are interested in the points (for example, in space) where this process crosses
 147 a level x_1 , the joint distribution of the space derivative of ξ_1 noted ξ_2 , with other related
 148 processes ξ_3, ξ_4, \dots at $\xi_1 = x_1$ is given by:

$$p(\xi_2, \xi_3, \xi_4, \dots)_{x_1} = \frac{|\xi_2| p(\xi_1, \xi_2, \xi_3, \xi_4, \dots)|_{\xi_1=x_1}}{N_0(x_1)} \quad (1)$$

149 where $N_0(x_1)$ is the number of crossings of the level x_1 by ξ_1 (see Equation 2.2.5 in Longuet-
 150 Higgins (1957)). In this paper we are interested in joint distributions at the local max-
 151 ima in space of the wave elevation process ξ_0 . Therefore, ξ_1 is the space derivative of the
 152 wave process and local maxima correspond to down-crossings of the zero level by $\xi_1 =$
 153 $\partial\xi_0/\partial x$.

$$\xi_1 = \frac{\partial\xi_0}{\partial x}, \quad \xi_2 = \frac{\partial^2\xi_0}{\partial x^2} = \frac{\partial\xi_1}{\partial x}. \quad (2)$$

154 In the case of Gaussian processes, $N_0^-(x_1)$ is:

$$N_0^-(x_1) = \frac{1}{2\pi} \sqrt{\frac{m_4}{m_2}} \exp\left(-\frac{x_1^2}{2m_2}\right), \quad N_0^- = N_0^-(0) = \frac{1}{2\pi} \sqrt{\frac{m_4}{m_2}} \quad (3)$$

155 where m_0, m_1, \dots, m_i are the i -th wavenumber spectral moments and the minus sign
 156 indicates that we consider only down-crossings.

157 **2.1.1 Speed of Local Maxima (Phase Speed)**

158 Following Longuet-Higgins (1957), if we are interested in the speed c of the local
 159 maxima in space, that is, the speed of the down-crossings of ξ_1 , we have:

$$c = -\frac{\partial\xi_1/\partial t}{\partial\xi_1/\partial x} = -\frac{\xi_3}{\xi_2} \text{ with } \xi_2 = \frac{\partial^2\xi_0}{\partial x^2} \text{ and } \xi_3 = \partial\xi_1/\partial t. \quad (4)$$

160 Using Equation 1,

$$p(\xi_2, \xi_3)_0 = \frac{|\xi_2| p(\xi_1, \xi_2, \xi_3)|_{\xi_1=0}}{N_0} \tag{5}$$

161 with $p(\xi_1, \xi_2, \xi_3)$ the point joint distribution of the three Gaussian processes $\frac{\partial \xi_0}{\partial x}$, $\frac{\partial^2 \xi_0}{\partial x^2}$, $\frac{\partial^2 \xi_0}{\partial x \partial t}$
 162 is:

$$p(\xi_1, \xi_2, \xi_3) = p(\xi_1) p(\xi_2, \xi_3) = \frac{e^{-\frac{\xi_1^2}{2m_2}}}{2\pi\sqrt{m_2}} e^{-\frac{1}{2} \begin{bmatrix} \xi_2 \\ \xi_3 \end{bmatrix} [\xi_2 \xi_3] Q_c^{-1} \begin{bmatrix} \xi_2 \\ \xi_3 \end{bmatrix}} \sqrt{(2\pi)^3 \det(Q_c)} \tag{6}$$

163 and covariance matrix:

$$Q = \begin{bmatrix} m_2 & 0 & 0 \\ 0 & m_4 & m'_3 \\ 0 & m'_3 & m''_2 \end{bmatrix} = \begin{bmatrix} m_2 & 0 \\ 0 & Q_c \end{bmatrix}. \tag{7}$$

164 Note that following Longuet-Higgins (1957) notations, m''_i indicates the mixed wavenumber-
 165 frequency i -th spectral moment, where the number of quotes indicates the order of the
 166 frequency spectral moment, for example,

$$m'_3 = \int_0^\infty 2\pi f^1 k^3 E(k) dk, \tag{8}$$

167 where $E(k)$ is a given wavenumber spectra.

168 Classically, to introduce c in the joint density and obtain $p(c, \xi_3)_0$, we apply a change
 169 of variables

$$\xi_2 = -\frac{\xi_3}{c}, \quad \xi_3 = \xi_3 \tag{9}$$

170 and after the integration of $p(c, \xi_3)_0$ over all the domain of definition of ξ_3 , we obtain
 171 the distribution of c (Longuet-Higgins (1957), Eq. 2.5.19):

$$p(c)_0 = \frac{1}{2} \frac{m_4 m_2'' - m_3'^2}{\sqrt{m_4} (c^2 m_4 + 2cm'_3 + m_2'')^{3/2}} \tag{10}$$

172 Note that the sign on c (or on m'_3) depends on the convention on the wave propagation
 173 direction. We have kept the convention used by Longuet-Higgins (1957) here.

174 **2.1.2 Introducing the Orbital Velocity**

175 As indicated in Equation 1, we can introduce in the formula a variable which rep-
 176 represents the horizontal orbital velocity. For Gaussian waves the horizontal orbital veloc-
 177 ity u is defined as

$$u = \mathcal{H}_t \left(\frac{\partial \xi_0}{\partial t} \right) \tag{11}$$

178 with \mathcal{H}_t the Hilbert transform in time domain. Which means that

$$\xi_0 = \sum_i a_i \cos(k_i x - \omega_i t) \tag{12}$$

179 is transformed in

$$u = \sum_i a_i \omega_i \cos(k_i x - \omega_i t), \tag{13}$$

180 with a_i the wave amplitude, k_i the wavenumber and ω_i the angular wave frequency of
 181 the wave component i . As the Hilbert transform is a linear operator, u is also Gaussian.

182 As previously, at the local maxima we have:

$$p(\xi_2, \xi_3, u)_0 = \frac{|\xi_2| p(\xi_1, \xi_2, \xi_3, u)|_{\xi_1=0}}{N_0^-} \tag{14}$$

183 with a new covariance matrix for ξ_1, ξ_2, ξ_3 and u :

$$Q = \begin{bmatrix} m_2 & 0 & 0 & 0 \\ 0 & m_4 & m'_3 & m'_2 \\ 0 & m'_3 & m''_2 & m''_1 \\ & m'_2 & m''_1 & m''_0 \end{bmatrix} = \begin{bmatrix} m_2 & 0 \\ 0 & Q_c \end{bmatrix}. \tag{15}$$

184 As previously, we can apply a similar change of variables

$$\xi_2 = -\frac{\xi_3}{c}, \quad \xi_3 = \xi_3, \quad u = u, \tag{16}$$

185 or the easiest to deal with,

$$\xi_3 = -c\xi_2, \quad \xi_2 = \xi_2, \quad u = u \tag{17}$$

186 and integrate $p(c, \xi_2, u)_0$ over all the domain of definition of ξ_2 . The result is a more com-
 187 plicated but again semi-analytical. The body of the integral has the form

$$e^{-\frac{1}{2}[\xi(c)\xi_2^2 + \beta(c,u)\xi_2 + \alpha(u)]\xi_2^2} \tag{18}$$

188 and its integration in ξ_2 on the down-crossings space $]-\infty, 0]$ gives

$$I(c, u) = \frac{\left((2\phi^2 + 1) \sqrt{\pi} (\operatorname{erf}(\phi) + 1) e^{\phi^2 + 2\phi} \right)}{\sqrt{2}\xi^{3/2}(c)} e^{-\alpha/2} \tag{19}$$

189 with

$$\phi = \phi(c, u) = \frac{1}{2\sqrt{2}} \frac{\beta(c, u)}{\sqrt{\xi(c)}}, \quad \alpha = \alpha(u), \tag{20}$$

$$\Delta = \det(Q_c) = m'_3 (m'_2 m''_1 - m'_3 m''_0) + m_4 (m''_0 m''_2 - m''_1{}^2) + m'_2 (m'_3 m''_1 - m'_2 m''_2), \tag{21}$$

$$\alpha(u) = \frac{m_4 m''_2 - m_3{}^2 u^2}{\Delta}, \tag{22}$$

$$\beta(c, u) = 2 \frac{m'_3 m''_1 - m'_2 m''_2}{\Delta} u + 2 \frac{m_4 m''_1 - m'_2 m'_3}{\Delta} u c \tag{23}$$

190 and

$$\xi(c) = \frac{m''_0 m''_2 - m''_1{}^2}{\Delta} + 2 \frac{m'_3 m''_0 - m'_2 m''_1}{\Delta} c + \frac{m_4 m''_0 - m_2{}^2}{\Delta} c^2. \tag{24}$$

191 The joint probability density of (c, u) is then:

$$p(c, u) = \frac{1}{N_0^-} \frac{1}{(2\pi)^2 \sqrt{m_2 \Delta}} I(c, u) = \frac{I(c, u)}{2\pi \sqrt{m_4 \Delta}}. \quad (25)$$

192 Note again that the sign on c and u (or on m'_2 and m'_3) depends on the convention on
 193 the wave propagation direction and Longuet-Higgins (1957)'s convention is still used here.
 194 The coefficients (α, β, ξ) can be calculated directly numerically and Δ is the determi-
 195 nant of Q_c , the sub-matrix of Q , and after the inverse of Q_c is calculated:

$$Q_c^{-1} = \begin{bmatrix} R & \mathbf{s} \\ \mathbf{s}^t & r \end{bmatrix} \quad (26)$$

196 we find

$$\alpha(u) = ru^2, \quad (27)$$

$$\beta(c, u) = 2 \begin{bmatrix} 1 & c \end{bmatrix} \mathbf{s}u, \quad (28)$$

$$\xi(c) = \begin{bmatrix} 1 & c \end{bmatrix} R \begin{bmatrix} 1 \\ c \end{bmatrix}. \quad (29)$$

197 An example of the joint density of the couple (phase speed, horizontal particle velocity)
 198 at local maxima in space is shown in Figures 1-a and b for a JONSWAP spectrum.

199 **2.2 Modelling P_b from $p(c, u)$**

200 By using Equation 25 applied to the dominant spectral wave band (that is, that
 201 contained in the interval $[0.7f_p, 1.3f_p]$, where f_p is the peak wave frequency), the prob-
 202 ability of dominant wave breaking can be computed by integrating Equation 25 over all
 203 phase speeds and for orbital velocities over a threshold Ac , with A a constant that will
 204 be in the next section:

$$P_b = \int_{u > Ac} \int_0^\infty p(c, u) dc du. \quad (30)$$

205 P_b will be modelled following Equation 30 hereafter. Note that from the definitions in
 206 Equation 3, the proposed P_b is defined as number of breaking local maxima over the to-

tal number of local maxima. From the analysis of $p(c, u)$ we observed that spurious, non-
 moving local maxima may exist around $c = 0$ and $u = 0$; therefore, to avoid artificially
 increasing P_b , we adopted a practical integration range of $c, u \in [0.05, +\infty]$ here. Note
 that this range may, however, only be valid for very narrow spectra. Further, we draw
 attention that, following from Equation 1, our P_b model is defined in space domain, whereas
 all the previous P_b models and data are (at least partially) defined in time domain (see
 Appendix A for details). For the very narrow spectral band used here, the differences
 between temporal and spatial definitions of P_b are negligible. This is discussed further
 in Section 5.

Finally, the proposed model can be extended to accommodate two-dimensional spec-
 tra without changes on how $p(c, u)$ is calculated. This is done by applying an appropri-
 ated spreading function to any given one-dimensional spectra (or directly inputting a di-
 rectional spectra) and by recalculating the moments in Equations 8 to take direction-
 ality into account or, more explicitly,

$$m_i = \int_0^{2\pi} \int_0^\infty (f \cos \theta \cos \alpha + f \sin \theta \sin \alpha)^i E(f, \theta) df d\theta. \quad (31)$$

An example considering the simplified cosine spreading law ($D(\theta) = \cos(\theta - \bar{\theta})^{2s}$) with
 $s = 20$, $\bar{\theta} = 0$ and $\alpha = 0$ applied to same JONSWAP spectrum shown in Figure 1-a is shown
 in Figure 1-c. Note that the differences in $p(c, u)$ between the one-dimensional (Figure
 1-b) and the two-dimensional (Figure 1-d) spectra are negligible for the present assump-
 tions. This relatively simple extension allows for the consideration of two-dimensional
 wave spectral but we caution the reader that it may not be fully complete. A follow-up
 publication will be dedicated to include and assess the effects of wave directionality in
 our method more rigorously.

2.3 Definition of a Gaussian-equivalent Non-linear Wave Breaking Cri- terion

The previously introduced joint probability density distribution $p(c, u)$ is based on
 Gaussian theory and therefore assumes that waves are linear. Breaking waves are, how-
 ever, highly non-linear. For real non-linear waves, as detailed in the introduction, it is
 widely accepted that wave breaking starts when the water particle horizontal velocity
 at its crest (u_{nl}) reaches the wave phase speed (c_{nl}). A non-linear wave breaking crite-

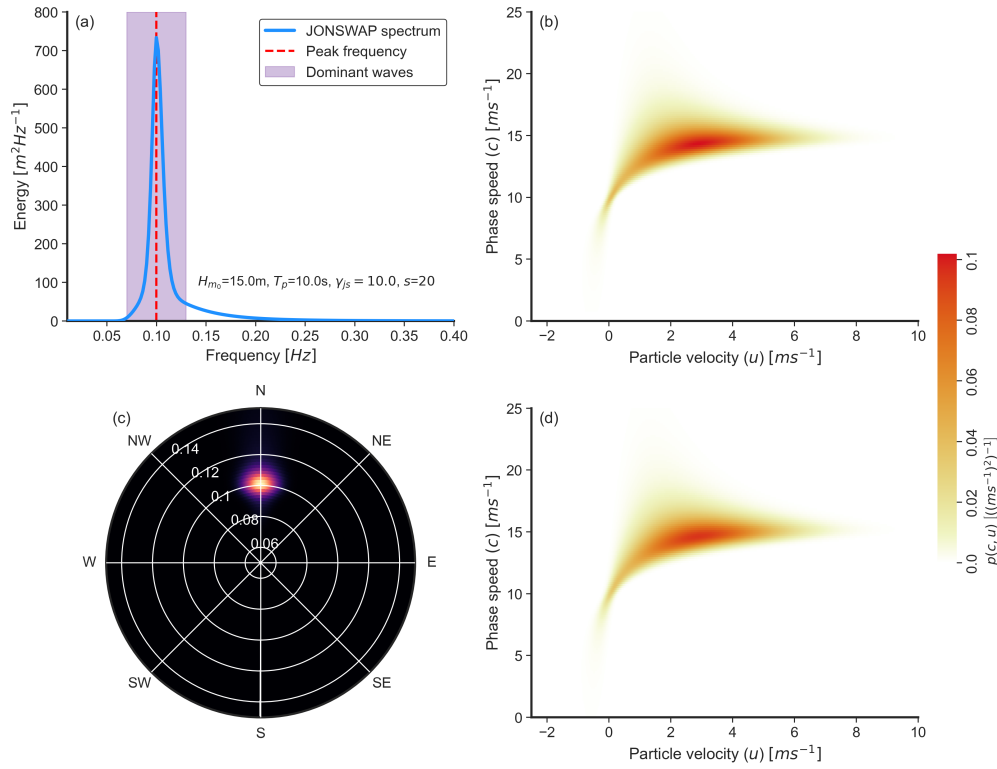


Figure 1. Example of the application of the method. a) JONSWAP spectrum for $H_{m_0}=15\text{m}$, $T_p=10\text{s}$ and shape parameter $\gamma_{js}=10$. b) Obtained joint probability density between the wave phase speed (c) and the horizontal particle velocity at wave crest (u) calculated using Equation 25. Note that the joint probability density was computed using only the spectral energy between $0.7f_p$ and $1.3f_p$, that is, corresponding to the dominant wave band only. c) Directional spectrum for the same parameters as in a) and directional spreading $D(\theta) = \cos(\theta - \bar{\theta})^{2s}$ with $s = 20$ and $\bar{\theta} = 0$. d) Obtained $p(c, u)$ considering only the spectral energy in the direction $\alpha = 0$.

236 rion can be thus be defined as $A_{nl} = u_{nl}/c_{nl} = 1$. Therefore, we assume that it is possible to obtain an equivalent kinematic criterion, $A_{lin} = constant$ that relates Gaussian
 237 waves to non-linear waves.
 238

239 Based on numerical experiments, Cokelet (1977) provided the potential and kinetic energy of a fully non-linear regular wave in deep-water at the onset of wave breaking (see
 240 the last row of his Table A.0). Based on his results, we define the kinematic criterion as the linear wave that has total energy equals to the nearly breaking non-linear regular
 241 wave computed by Cokelet (1977). Following Cokelet (1977), where k , g and ρ are expressed as non-dimensional variables, a deep-water wave at the breaking onset (see last
 242 row of his table A.0) has kinetic energy $T = 3.827 \times 10^{-2}$ and potential energy $V = 3.457 \times 10^{-2}$. The energy-equivalent linear wave (denote with subscript eq) has, therefore, amplitude:
 243
 244
 245
 246
 247

$$a_{eq} = \sqrt{2 \times E} = \sqrt{2 \times (V + T)} = 0.3817. \quad (32)$$

248 For this particular case, the linear dispersion relation reads:

$$\omega^2 = gk = 1, \quad (33)$$

249 the fluid velocity at crest of the energy-equivalent linear wave is:

$$u_{eq} = \omega a_{eq} = 0.3817, \quad (34)$$

250 and the phase speed of the linear wave is:

$$c_{eq} = \sqrt{\frac{g}{k}} = 1. \quad (35)$$

251 Given these constants, we obtain:

$$A_{lin} = \frac{u_{eq}}{c_{eq}} = \frac{0.3817}{1} = 0.3817. \quad (36)$$

252 Following this approach, we define the correction coefficient $A = A_{lin} = 0.382$ that
 253 will be used as reference value hereafter for our tests. This result is consistent with re-

254 cent findings from Ardag and Resio (2020) who reported from the re-analysis of Duncan’s
 255 (1981) experimental results, a wave breaking threshold between 0.75 and 1.02 (see their
 256 Figure 1). Note, however, that these authors defined their wave breaking threshold as
 257 u/c_g , where c_g is the group velocity and u was obtained from linear wave theory. Replac-
 258 ing wave group velocity (c_g) by the wave phase speed (c) yields a range of possible val-
 259 ues between 0.35 and 0.50, which is consistent with A_{lin} .

260 Figure 2 illustrates the sensitivity in wave breaking probability with changes in the
 261 wave breaking threshold A . For the given $p(c, u)$ in Figure 2-a, letting A to vary from
 262 0 to 1 resulted in a exponential increase in P_b at $A \leq 0.2$ (Figure 2-b), which may be
 263 unrealistic. When setting $A=A_{lin}=0.382$ and letting the significant wave height (H_{m_0})
 264 and wave peak period (T_p) vary in the definition of the JONSWAP spectrum, the results
 265 indicate that steeper waves are more probable to break, which is expected (Figure 2-c).
 266 Finally, note that the wave breaking threshold A might be sensitive to other wave and
 267 atmospheric parameters such as wave directionality or direct wind forcing (or, equiva-
 268 lently, wave age). In the next sections, the accuracy of our model is assessed using field
 269 observations and our results are compared with other parametric wave breaking formu-
 270 lations.

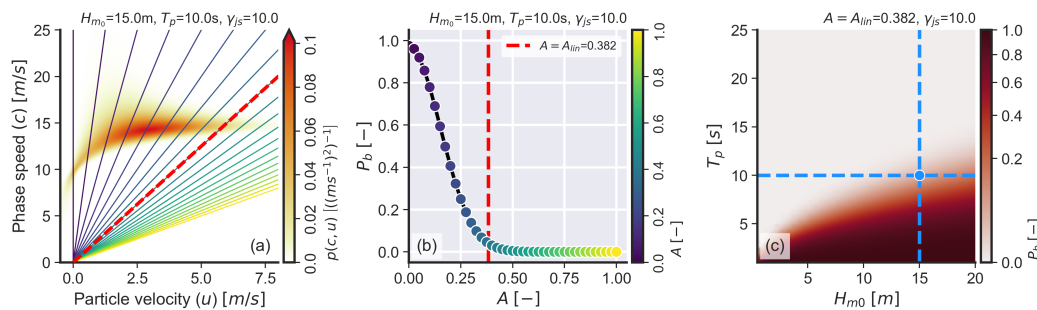


Figure 2. a) Example of joint probability density between u and c obtained from Equation 30. The colored lines indicate different values of A and the red dashed line shows $A=A_{lin}=0.382$. b) Possible values of P_b for varying A calculated using the joint PDF from a). The vertical dashed line shows $A=A_{lin}=0.382$. c) Obtained P_b for varying H_{m_0} and T_p and fixed A (0.382) and γ_{js} (10). The dashed blue lines and marker indicate the H_{m_0} and T_p values used in a) and b). Note that as in Figure 1, these results only consider dominant waves, that is, they were calculated from the spectrum between $0.7f_p$ and $1.3f_p$.

271 **3 Field Data**

272 Three historical datasets were used to evaluate the present model. Further, six his-
273 torical models (detailed in Appendix A) were chosen to contextualize our model in re-
274 lation to the state-of-the-art. These historical models range from baseline models in which
275 the only inputs are known environmental parameters (wind speed in Melville and Ma-
276 tusov (2002) or wave steepness in Banner et al. (2000), for example) to fairly complex
277 models that account for combinations of several phenomena (Romero (2019), for exam-
278 ple).

279 **3.1 Thomson (2012) and Schwendeman et al. (2014) dataset (TSG14)**

280 The first data are from Thomson (2012) and Schwendeman et al. (2014), hereafter
281 TSG14, and were collected in the Strait of Juan de Fuca, Washington. These data were
282 collected by a gray scale video camera with a resolution of 640×480 pixels installed above
283 the wheelhouse of Research Vessel R/V *Robertson* which recorded at an acquisition rate
284 of 30 Hz (Schwendeman et al., 2014). These data were then projected into a metric co-
285 ordinate grid with resolution of 0.25m (cross wave) and 0.075m (along wave) using the
286 method proposed by Holland et al. (1997) and were then used to obtain $\Lambda(c)$ using the
287 spectral approach of Thomson and Jessup (2009). The data were collected in a (usually)
288 fetch-limited region and for a young sea state; note, however, that the particular sea-states
289 analyzed here may not be fetch-limited. Figure 3-a shows the measured wave spectra,
290 Figure 3-b shows $\Lambda(c)$ distributions, and Table 1 shows a summary of these data. For
291 these data, P_b was calculated using the measured $\Lambda(c)$ distributions combined with the
292 method described below in Equation 37. Additional information regarding the data col-
293 lection is available from Thomson (2012) and Schwendeman et al. (2014).

294 **3.2 Sutherland and Melville (2013) dataset (SM13)**

295 The second dataset is from Sutherland and Melville (2013), hereafter SM13, and
296 was collected using the Research Platform R/P *FLIP* during a two-day field campaign
297 in the Southern California Bight under the scope of the SoCal 2010 experiment (Sutherland
298 & Melville, 2013). Here, we focus only on the visible imagery collected by these authors
299 to keep consistency with the previously presented data. Stereo video data were collected
300 by a pair of video cameras mounted on the R/P FLIP for 10 minutes at the start of each

hour and $\Lambda(c)$ was obtained using a variation of the method of Kleiss and Melville (2011), that is, tracking the temporal evolution of breakers obtained via pixel intensity threshold. Figure 3-c shows the measured wave spectra, Figure 3-d shows $\Lambda(c)$ distributions, and Table 1 shows a summary of these data. Note that because wave breaking was not observed for frequencies below $0.2Hz$ and from numerical simulations (not shown) these waves corresponded to a cross-swell not forced by the wind, our analyses only consider waves in the frequency range $0.2 < f < 0.8Hz$. Additional information regarding the data collection is available from Sutherland and Melville (2013). For these and TSG14 data, P_b was calculated using the measured $\Lambda(c)$ distributions combined with the formulas from Banner and Morison (2010):

$$P_b = \frac{\int_{c_0}^{c_1} c\Lambda(c)dc}{\int_{c_0}^{c_1} c\Pi(c)dc} \quad (37)$$

where $c_0 = \frac{g}{2\pi} \frac{1}{1.3f_p}$, $c_1 = \frac{g}{2\pi} \frac{1}{0.7f_p}$, $\Pi(c) = \chi g / (2\pi c^3)$ and $\chi = 0.6$. The implication of this choice is discussed in further detail in Section 5.

3.3 Banner, Babanin and Young (2000) dataset (B00)

The third dataset is from Banner et al. (2000), hereafter B00, and was collected in the Black Sea (BS), Lake Washington (LW) and the Southern Ocean (SO). These authors directly provide values for significant wave height H_{m0} , peak period (T_p) and the wave breaking probability in their Tables 1 (Black Sea, denoted as BS here) and 2 (Southern Ocean, denoted as SO here). The majority of the data were collected in the Black Sea (13 data runs) and two data runs are from the Southern Ocean. Given that the original spectral data were not published alongside their paper, we approximate the observed spectra using the provided pairs H_{m0} , T_p assuming a JONSWAP shape with $\gamma_{js} = 3.3$ (as previously done in Filipot et al. (2010), for example). Given that in this paper we are only interested in a very narrow spectral band, the differences between observed and simulated spectra should be minimal. For more details regarding this data refer to Banner et al. (2000).

Table 1. Data summary for the two experiments described in Sections 3.1 and 3.2. Note that the parameters obtained from wave spectra were computed specifically for the bands shown in Figure 3 for TSG14 and SM13 cases. The wave height (H_p) and wave steepness (ϵ) parameters for dominant waves were calculated as per Banner et al. (2002) (see Section A1 for details). The wave age parameter was calculated as c_p/u_* .

Dataset	Date	Length	H_{m_0}	T_p	H_p	ϵ	U_{10}	u_*	c_p	Wave age	P_b
	[–]	[min]	[m]	[s]	[m]	[–]	[ms^{-1}]	[ms^{-1}]	[ms^{-1}]	[–]	[–]
TSG14	14/02/2011 20:33	6.5	0.75	2.88	0.66	0.160	11.50	0.373	4.50	12.07	3.54E-03
TSG14	14/02/2011 20:58	5.1	0.75	2.96	0.66	0.152	12.55	0.417	4.62	11.08	9.57E-03
TSG14	14/02/2011 21:30	6.5	0.91	2.99	0.82	0.184	15.07	0.561	4.67	8.33	6.29E-02
TSG14	14/02/2011 21:44	8.5	1.09	3.17	1.00	0.200	15.73	0.599	4.94	8.25	1.01E-01
TSG14	14/02/2011 22:29	6	1.21	3.44	1.09	0.186	17.24	0.636	5.36	8.44	1.51E-01
TSG14	14/02/2011 22:37	4.8	1.37	3.53	1.24	0.199	18.01	0.660	5.52	8.36	7.61E-02
TSG14	15/02/2011 19:04	10	0.87	3.29	0.79	0.146	14.45	0.360	5.13	14.28	3.75E-03
TSG14	15/02/2011 19:19	6	0.90	3.31	0.81	0.149	13.11	0.477	5.17	10.85	4.05E-02
SM13	06/12/2010 21:59	10	0.61	3.51	0.52	0.085	6.46	0.205	5.48	26.68	7.96E-03
SM13	06/12/2010 23:00	10	0.61	3.33	0.54	0.097	7.55	0.342	5.20	15.22	1.95E-03
SM13	07/12/2010 00:00	10	0.73	3.45	0.66	0.112	8.62	0.319	5.38	16.85	3.24E-03
SM13	08/12/2010 00:00	10	0.34	2.04	0.23	0.110	5.24	0.160	3.19	19.96	1.65E-02
B00 (SO)	10/6/1992	5	9.20	13.46	8.02	0.089	19.80	0.835	21.01	25.17	2.70E-02
B00 (SO)	11/6/1992	9	4.20	12.04	3.66	0.051	16.00	0.626	18.78	30.02	0.00E+00
B00 (BS)	1993	34-68	0.39	2.78	0.34	0.089	11.70	0.414	4.34	10.49	3.80E-02
B00 (BS)	1993	34-68	0.49	2.94	0.43	0.100	12.70	0.461	4.59	9.96	6.50E-02
B00(BS)	1993	34-68	0.53	3.33	0.47	0.084	14.00	0.524	5.20	9.93	6.00E-02
B00 (BS)	1993	34-68	0.54	3.23	0.47	0.092	14.40	0.544	5.04	9.26	5.20E-02
B00 (BS)	1993	34-68	0.38	2.27	0.34	0.131	15.00	0.574	3.55	6.18	6.30E-02
B00 (BS)	1993	34-68	0.45	2.56	0.40	0.121	14.60	0.554	4.00	7.23	6.70E-02
B00 (BS)	1993	34-68	0.45	2.44	0.40	0.134	13.70	0.509	3.81	7.49	8.40E-02
B00 (BS)	1993	34-68	1.19	5.88	1.04	0.061	8.70	0.295	9.18	31.10	0.00E+00
B00 (BS)	1993	34-68	1.32	6.24	1.15	0.060	11.20	0.391	9.74	24.91	0.00E+00
B00 (BS)	1993	34-68	0.83	6.24	0.73	0.038	9.50	0.322	9.74	30.22	0.00E+00
B00 (BS)	1993	34-68	0.89	5.88	0.78	0.045	10.70	0.368	9.18	24.91	0.00E+00
B00 (BS)	1993	34-68	0.99	3.71	0.87	0.127	10.00	0.339	5.79	17.06	3.40E-02
B00 (BS)	1993	34-68	0.88	4.00	0.77	0.097	8.70	0.295	6.24	21.14	5.80E-02

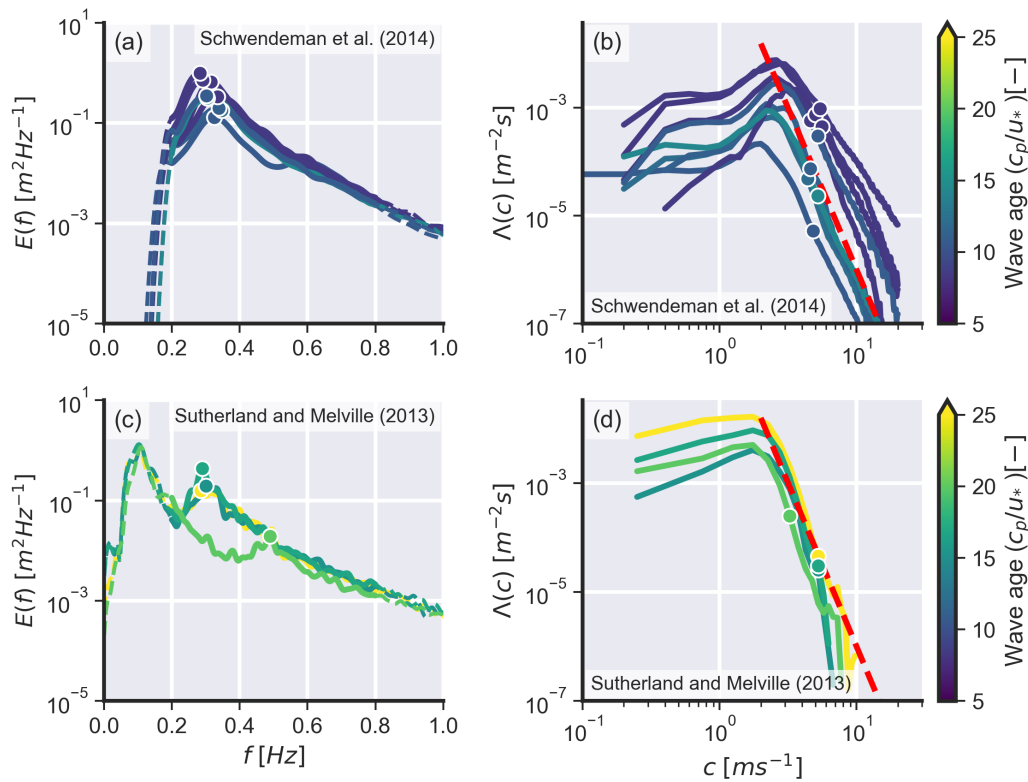


Figure 3. Field data. a) Spectral data from TSG14. b) $\Lambda(c)$ data from STG14. c) Spectral data from SM13. d) $\Lambda(c)$ data from SM13. The coloured circular markers show in a) and c) show the peak frequency (f_p) and the coloured circular markers show in b) and d) show the peak wave speed (c_p). The red dashed line in b) and d) shows the theoretical c^{-6} decay predicted by Phillips (1985). In all plots, the color scale shows the wave age (c_p/u_*).

326 **4 Results**

327 **4.1 Comparison with Field Data**

328 Figure 4 shows the comparison between estimated (or observed) (x-axis) and mod-
 329 elled (y-axis) values of P_b for each model. In general, no model was able to closely re-
 330 produce the trends seen in the combined observed data, regardless of the underlying math-
 331 ematical or physical formalism. Furthermore, orders of magnitude of difference between
 332 the models and, more worryingly, between the models and the measured data were ob-
 333 served. In general, models based on a wave steepness-derived wave breaking criterion (Banner
 334 et al. (2000), Banner et al. (2002), for example) overestimated data derived from $\Lambda(c)$
 335 while models based on $\Lambda(c)$ (Melville and Matusov (2002) and Sutherland and Melville
 336 (2013), for example) underestimated P_b data that was not derived from Λ (that is, B00
 337 data). The model from Filipot et al. (2010) was found to be the most consistent model.
 338 From Figure 4-g, the formulation presented in Section 2 with $A = A_{lin} = 0.382$ under-
 339 estimated the observed P_b for B00 and SM13 data (note that P_b was too low to be dis-
 340 played on the plot) but performed relatively well for the majority of TSG14 data. Us-
 341 ing the mean absolute error (MAE) as a convenient metric to assess the models, it was
 342 found that the present model has errors in the same order of magnitude as the previ-
 343 ous models. Given the spread in the results seen in Figure 4, no model could be consid-
 344 ered a clear winner. For the discussion of these results, see Section 5.

345 **4.2 Model Optimization**

346 From the analysis of Figure 2, minor changes in A can lead to major variations in
 347 P_b . Further, from the analysis of Figure 4, the proposed model underestimated P_b for
 348 $A = A_{lin} = 0.382$ particularly for S13 and B00 data. Given that it is a common prac-
 349 tice to optimize wave breaking models for particular datasets, we present two methods
 350 to do so using TSG14 data as an example. The same could be done for B00 and SM13
 351 data but, for brevity, this is not done here. Given that the present model is not compu-
 352 tationally expensive, the first approach consisted of varying A from 0.1 to 0.5 in 0.001
 353 intervals and finding the value of A that resulted in the lowest squared error ($\sqrt{(p_{b_i}^d - p_{b_i}^m)^2}$,
 354 where the superscripts d and m indicate observed and modelled data, respectively) for
 355 each data run. Figure 5-a shows the results of this procedure. The value $A = A_{opt} = 0.24$
 356 was, on average, the optimal values of for this particular dataset. The second approach

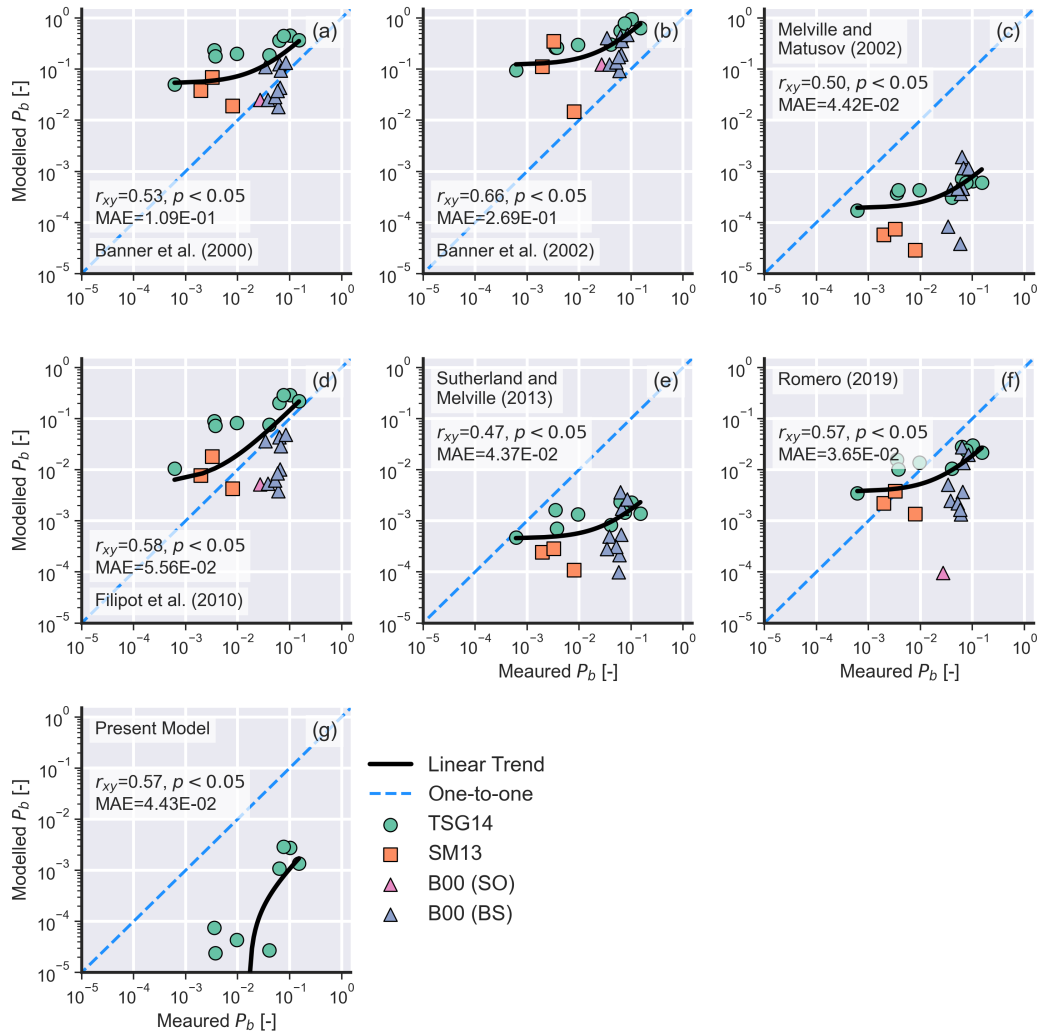


Figure 4. Comparison between measured and computed P_b for different models and data. a) Banner et al. (2000), b) Banner et al. (2002), c) Melville and Matusov (2002), d) Filipot et al. (2010), e) Sutherland and Melville (2013), f) Romero (2019), and g) present model with $A=A_{lim}=0.382$. The thick black line shows the linear regression between measured and modelled P_b and the blue dashed line indicates the one-to-one correspondence in all panels. Data points with modelled $P_b < 10^{-5}$ or observed $P_b = 0$ are not shown in this plot. In all plots, r_{xy} is Pearson’s correlation coefficient and MAE indicates the mean absolute error. Note the logarithmic scale.

357 consisted in parameterizing the optimal value of A for each data run as a function of a
 358 known environmental variable, in this example, the waveage c_p/u_* (Figure 5-b). The re-
 359 sults of these two approaches are show in Figures 5-c and d, respectively. Both approaches
 360 considerably improved the model results from the baseline model presented in Figure 4,
 361 with the parametric model (Figure 5-d) performing slightly better when considering Pear-
 362 son’s correlation coefficient (r_{xy}) as a comparison metric.

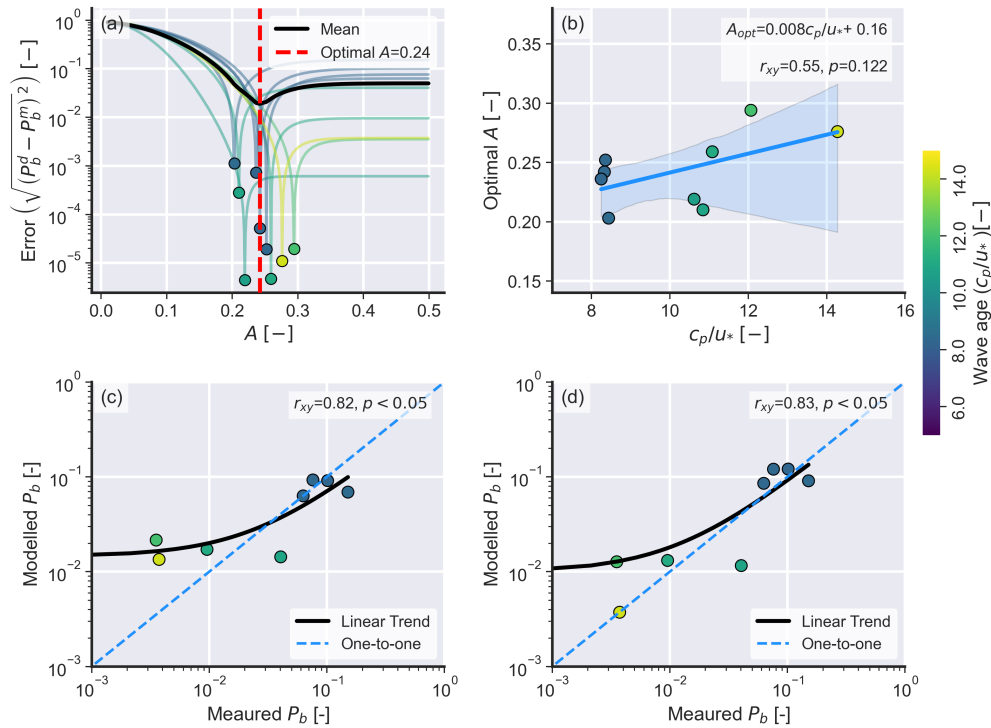


Figure 5. Results of the optimization procedures. a) Optimization curves for each data record (coloured lines) and the global averaged (black line). The vertical dashed line show $sA = A_{opt} = 0.24$. b) Parametrization of A as a function of c_p/u_* . The blue swath indicates the 95% confidence interval. For this particular case, $A = 0.008c_p/u_* + 0.16$. Note the logarithmic scale in a), c) and d). In all plots, the color scale shows the wave age (c_p/u_*). In b) to d) r_{xy} is Pearson’s correlation coefficient.

363 **5 Discussion**

364 We have introduced a new model for obtaining the probability of wave breaking
 365 (P_b) for dominant waves based on the theoretical joint probability density distribution
 366 between wave phase speed (c) and horizontal orbital velocity at the wave crest (u) for

367 unidirectional Gaussian wave fields. The present model has only one parameter for defin-
368 ing the wave breaking threshold (A), which makes it relatively easy to optimize for a given
369 dataset (as shown in Section 4.2). While the proposed model performed relatively well
370 for one of the investigated datasets (TSG14), it greatly underestimated P_b for the two
371 other datasets (SM13 and B00). For the data investigated here, such underestimation
372 did not result in a high mean absolute error (MAE) and, in fact, our model had one of
373 the lowest MAE. Recent results of Barthelemy et al. (2018), Derakhti et al. (2020) and
374 Varing et al. (2020) showed that waves with horizontal fluid velocity that exceeds 0.85
375 times the phase velocity will inevitably break. These results suggest that the breaking
376 threshold derived from Cokelet (1977) in Section 2.3 could be reduced by $\approx 15\%$. If we
377 apply their findings to our case, we obtain $A = 0.382 \times 0.85 = 0.324$ which would help
378 to reduce the underestimation of P_b , but not significantly. It is more probable that other
379 environmental phenomena such as direct wind forcing, directional spreading and long
380 wave modulation, which are not accounted in our model, are the reason for such differ-
381 ences.

382 One of the most challenging aspects when assessing our model is, nevertheless, re-
383 garding the field data. The attribution of wave breaking occurrences to wave scales us-
384 ing timeseries analysis, as done in Banner et al. (2000) or Filipot et al. (2010), is diffi-
385 cult because several wave scales can be present at the same time and space. This lead
386 us to use $\Lambda(c)$ observations as well as data from Banner et al. (2000) to investigate our
387 model. Different interpretations of how $\Lambda(c)dc$ is computed from field data can, how-
388 ever, generate orders of magnitude of difference in its moments (Gemmrich et al., 2013;
389 Banner et al., 2014) and, consequently, in P_b . Next, it is difficult to relate the speed of
390 the wave breaking front to the phase speed of the carrying wave because small, slower
391 breaking waves could merely be traveling on top of longer, much faster waves. In par-
392 ticular, we believe that these wave breaking events can significantly contribute to the ob-
393 served $\Lambda(c)dc$ distribution as they would have c close to the peak wave phase speed. This
394 wave breaking “sub-population” has not receive much research interest because of its ap-
395 parent small contribution to energy dissipation but, for our particular case, they directly
396 impact model validation.

397 Further, relating $\Lambda(c)$ to P_b is also challenging. Here, we adopted the convenient
398 formula from Banner and Morison (2010). While this formula has some support from
399 the literature (Ardhuin et al., 2010), the actual functional form of $\Pi(c)$ and the value

400 for the constant χ (see Equation 37) are unknown and changes in these will lead to changes
 401 in P_b . The Gaussian framework developed in Section 2.1 provides an alternative method
 402 to obtain $\Pi(c)$ (from Equation 3, for example) but this is beyond the scope of this in-
 403 troduutory paper and will be the focus of a future publication.

404 Finally, we would like to re-emphasize that our model is derived in the space do-
 405 main whereas P_b data is (at least partially) obtained in the time domain. For the nar-
 406 row spectral band investigated here, Monte-Carlo simulations of linear waves indicate
 407 that the difference between P_b modelled in space is less than five percent from P_b mod-
 408 elled in time (not shown). Given all these complications and the fact that some histor-
 409 ical models are being compared to data that was used to create them (Banner et al. (2000)
 410 and Sutherland and Melville (2013), for example), we are unable to provide an accurate
 411 ranking of the existing models. Future research should focus, therefore, on obtaining P_b
 412 data that is unambiguous and widely available. In this regard, and despite its own lim-
 413 itations, wave tank experiments could bring further insight on the statistics of dominant
 414 (or not) breaking waves. Such a dataset would ultimately allow researchers to focus on
 415 models derived from physical and mathematical concepts (such as ours) rather than on
 416 empirical concepts.

417 **6 Conclusion**

418 We have presented a new statistical wave breaking model derived from Gaussian
 419 field theory that we have applied to obtain the probability of wave breaking for domi-
 420 nant, wind-sea waves. Although more mathematically complex than previous formula-
 421 tions, the present model relies on the ratio between the crest orbital velocity and the phase
 422 speed and uses only on a single free parameter, the wave breaking threshold A . Using
 423 theoretical results obtained by Cokelet (1977) for regular nearly breaking waves, we de-
 424 rived a wave breaking threshold to adapt our linear model to non-linear waves. The present
 425 model has errors in the same order of magnitude as six other historical models when as-
 426 sessed using three field datasets. For a particular dataset (TSG14), our model performed
 427 well, especially if the free-parameter A is fine tuned. Additional observations are how-
 428 ever required, to further understanding and quantifying the dependence of A on envi-
 429 ronmental parameters that are not accounted for in our model (for example, wind forc-
 430 ing, wave directionality or modulation by long waves). Future research should be ded-
 431 icated to collect more wave breaking observations in different and repeatable environ-

432 mental conditions to provide reliable constraints for the optimization of the present and
 433 other wave breaking models. Still and although the research presented here is in early
 434 stages, the present model should be extendable to waves of any scale and, therefore, has
 435 the potential to be implemented in current state-of-the-art spectral wave models as a new
 436 wave breaking dissipation source term with relatively little effort.

437 **Appendix A Historic Parametric Wave Breaking Models**

438 **A1 Banner et al. (2000)**

439 Banner et al.'s (2000) is a popular model for calculating wave breaking probabil-
 440 ities for deep water, dominant waves. This model follows from observations and results
 441 from Donelan et al. (1972), Holthuijsen and Herbers (1986) and Banner and Tian (1998)
 442 who demonstrated the importance of the wave group modulation on the wave breaking
 443 onset. These authors conveniently obtained a parameterization for the probability of wave
 444 breaking (P_b) based solely on the spectral steepness of the dominant wave scale (ϵ_p), as-
 445 suming that their formulas would capture the influence of the wave group modulation
 446 on the wave breaking onset. Their formulation was derived using a dataset of measure-
 447 ments collected in various environments ranging from lakes to open ocean conditions (Banner
 448 et al., 2000). From these observations, these authors were then able to obtain a wave break-
 449 ing threshold behaviour for the dominant waves as a function of the dominant spectral
 450 wave steepness given by:

$$\epsilon_p = \frac{H_p k_p}{2} \tag{A1}$$

451 in which k_p is the wavenumber at peak frequency (f_p) and H_p is the significant wave height
 452 of the dominant waves calculated as:

$$H_p = 4 \sqrt{\left(\int_{0.7f_p}^{1.3f_p} E(f) df \right)} \tag{A2}$$

453 where $E(f)$ is the spectra of wave heights as a function of frequency. For their data, P_b
 454 was then parameterized as a single equation with three free parameters (p_1, p_2, p_3):

$$P_b = p_1 + (\epsilon_p - p_2)^{p_3}, \tag{A3}$$

455 For the available field data, Banner et al. (2000) found optimal values of $p_1 = 22$, $p_2 =$
 456 0.055 , and $p_3 = 2.01$. Note that hereafter free parameters for the different models will
 457 be denoted as p_n where n is a sequential number.

458 **A2 Banner et al. (2002)**

459 This work extended Banner et al. (2000) model to shorter wave scales (up to 2.48
 460 times the peak wave frequency). From field data Banner et al. (2002) reported that the
 461 waves were breaking if the saturation spectrum $\sigma(f) = 2\pi^4 f^5 E(f)/2g^2 = \sigma(k) = k^4 E(k)$
 462 exceeded a threshold that was frequency dependent. These author's related this depen-
 463 dence to the directional spreading $\overline{\theta(k)}$ which later led Banner and Morison (2010) to
 464 explicitly define the following empirical formulation:

$$P_b(k_c) = \mathcal{H}_h(\tilde{\sigma}(k_c) - p_1) \times p_2 \times (\tilde{\sigma}(k_c) - \tilde{\sigma}_t), \quad (\text{A4})$$

465 in which \mathcal{H}_h is the Heaviside step function, k_c is the central wavenumber for a given wavenum-
 466 ber range, $\tilde{\sigma}(k_c) = \sigma(k_c)/\overline{\theta(k_c)}$ is the saturation spectrum normalized by the averaged
 467 directional spreading, $p_1 = 0.0045$ and $p_2 = 33$ are constants obtained from their ob-
 468 servations. Following Banner et al. (2002), the directional spreading angle is calculated
 469 according to Hwang et al. (2000) (their equation 19a):

$$\theta\left(\frac{k}{k_p}\right) = \begin{cases} 0.35 + 1.05\left(1 - \frac{k}{k_p}\right) & \text{if } \frac{k}{k_p} < 1.05 \\ 0.30 + 0.087\left(\frac{k}{k_p} - 1\right) & \text{if } 1.05 \leq \frac{k}{k_p} < 5 \end{cases} \quad (\text{A5})$$

470 where θ is the directional spreading angle as a function of the wavenumber.

471 **A3 Filipot et al. (2010)**

472 This method follows from the original works of Le Méhauté (1962), Battjes and Janssen
 473 (1978) and Thornton and Guza (1983) and assumes that the probability distribution func-
 474 tion (PDF) of breaking wave heights in the dominant wave scale is parameterized by its
 475 central frequency f_c or, equivalently, by its representative phase speed $c(f_c)$ and the prod-
 476 uct between a Rayleigh PDF for the wave heights

$$P(H, f_c) = \frac{2H}{H_{rms}^2(f_c)} \exp \left[- \left(\frac{H}{H_{rms}(f_c)} \right)^2 \right] \quad (A6)$$

477 in which

$$H_r(f_c) = \frac{4}{\sqrt{2}} \sqrt{\int_0^\infty U_{f_c}(f) E(f) df} \quad (A7)$$

478 and

$$U_{f_c} = 0.5 - 0.5 \cos \left(\frac{\pi}{\delta} \left[\frac{f}{f_c} - 1 - \delta \right] \right) \quad (A8)$$

479 where δ is the bandwidth of a Hann window (in this study, $\delta = 0.6$), and a weighting
480 function

$$W(H, f_c) = p_1 \left[\frac{\beta_r}{\beta} \right]^2 \left\{ 1 - \exp \left[- \left(\frac{\beta}{\tilde{\beta}} \right)^{p_2} \right] \right\} \quad (A9)$$

481 in which $\beta = kH / \tanh(kh)$, and p_1 and p_2 are free parameters. In order to extend the
482 formulation outside the shallow water domain, these authors replaced Thornton and Guza's
483 (1983) breaking criterion based on the wave height (H) to water depth (h) ratio ($\gamma =$
484 $H/h = 0.42$) with an adaptation of Miche's (1944) wave breaking parameter:

$$\beta_r = \frac{\overline{k_r}(f_c) H_r(f_c)}{\tanh(\overline{k_r}(f_c) h)} \quad (A10)$$

485 in which

$$\overline{k_r}(f_c) = \frac{\int_0^\infty U_{f_c}(f) k(f) E(f) df}{\int_0^\infty U_{f_c}(f) E(f) df} \quad (A11)$$

486 and

$$\tilde{\beta} = b(b_3 \tanh(kh)^3 - b_2 \tanh(kh)^2 + b_1 \tanh(kh) - b_0) \quad (A12)$$

487 in which $b = 0.48$, $b_3 = 1.0314$, $b_2 = 1.9958$, $b_1 = 1.5522$, and $b_0 = 0.1885$. In their
488 model, the variable $\tilde{\beta}$ was obtained via numerical calculations of regular nearly break-

489 ing waves using the stream wave theory of Dean (1965). Finally, the wave breaking prob-
 490 ability is obtained as:

$$P_b(f_c) = \int_0^\infty P(H, f_c)W(H, f_c)dH \leq 1. \quad (\text{A13})$$

491 To keep consistency with Section A2, P_b will be only considered at the spectral peak;
 492 other definitions are, however, also possible.

493 **A4 Models based on Phillips’ (1985) $\Lambda(c)$**

494 The major issue with the previous models is the difficulty to obtain reliable obser-
 495 vations of the wave breaking probabilities as a spectral distribution solely from point mea-
 496 surements. Due to the presence of different wave scales at the time and location, it is
 497 indeed difficult to assign the breaking occurrence to a given wave frequency of wave num-
 498 ber. To avoid this problem, Phillips (1985) proposed to use the speed of the breaking
 499 front as a proxy for the phase speed of the carrying wave. Phillips (1985) defined the pa-
 500 rameter $\Lambda(c)dc$ as the “average total length per unit surface area of breaking fronts that
 501 have velocities in the range c to $c + dc$ ” and then defined the following quantities:

$$L = \int \Lambda(c)dc \quad (\text{A14})$$

502 and

$$R = \int c\Lambda(c)dc \quad (\text{A15})$$

503 which represent the “total length of breaking fronts per unit area” (Equation A14) and
 504 “the total number of breaking waves of all scales passing a given point per unit time”
 505 (Equation A15). Assuming that Phillips (1985) assumptions hold, it is possible to ob-
 506 tain parametric models for Λ from known variables (e.g., wind speed) and, consequently,
 507 for P_b (see Equation 37).

508 **A41 Melville and Matusov (2002)**

509 Melville and Matusov’s (2002) model for $\Lambda(c)$ relies only on the wind speed mea-
 510 sured at 10m (U_{10}) to obtain $\Lambda(c)$. Following Melville and Matusov (2002) and using

511 the explicit formula given by Reul and Chapron (2003), this parameterization is writ-
 512 ten as:

$$\Lambda(c) = p_1 \left[\frac{U_{10}}{10} \right]^3 10^{-4} \exp[-(p_2 c)] \quad (\text{A16})$$

513 in which p_1 and p_2 are constants. For their data, Melville and Matusov (2002) found $p_1 =$
 514 3.3 and $p_2 = 0.64$. As discussed by Reul and Chapron (2003), this formulation approaches
 515 Phillips's (1985) theoretical c^{-6} but may overly estimates the amount of small breakers.

516 ***A42 Sutherland and Melville (2013)***

517 Sutherland and Melville (2013) used dimensional analysis to scale $\Lambda(c)$ and obtain
 518 a parameterization that is a function of the wind drag (u_*), peak wave phase speed (c_p),
 519 significant wave height (H_s) and three constants. From Sutherland and Melville's (2013)
 520 Equation 9 and their Figure 4, $\Lambda(c)$ is calculated as:

$$\Lambda(c) = p_1 \frac{g}{c_p^3} \left(\frac{u_*}{c_p} \right)^{p_2} \left(\frac{c}{\sqrt{gH_s}} \left(\frac{gH_s}{c_p^2} \right)^{p_3} \right)^{-6} \quad (\text{A17})$$

521 where $p_1 = 0.05$, $p_2 = 0.5$, and $p_3 = 0.1$ are constants obtained from the available data.
 522 Their formulation reproduces Phillips's (1985) c^{-6} frequency dependency but does not
 523 have the typical roll-off at low c as these authors chose to use infrared (other than vis-
 524 ible) imagery to obtain and model their $\Lambda(c)$. This choice included the contribution of
 525 micro-scale breakers that do generate visible bubbles in their model, hence the difference.

526 ***A43 Romero (2019)***

527 Recently, Romero (2019) developed and implemented a new wave breaking param-
 528 eterization in WaveWatchIII which relies exclusively on $\Lambda(c)$. Differently from previous
 529 parameterizations, Romero's (2019) takes into account both the modulations due to winds
 530 and long waves on $\Lambda(c)$. His model is fairly general but depends on six free parameters
 531 that needed to be laboriously obtained by comparing WaveWatchIII's significant wave
 532 height outputs with available measured significant wave heights from buoy data. In Romero's
 533 (2019) model, Λ was modelled assuming that it is proportional to the crest lengths ex-
 534 ceeding a slope threshold:

$$\Lambda(f, \theta) = \left(\frac{2(2\pi)^2 p_1}{g} \right) f \exp \left[- \left(\frac{p_2}{B(f, \theta)} \right) \right] M_{LW} M_W \quad (\text{A18})$$

535 where $p_1 = 3.5 \times 10^{-5}$ and $p_2 = 5 \times 10^{-3}$ are constants to be obtained from the data, M_{LW}
 536 is the modulation due to long waves, M_W is the modulation due to winds and $B(f, \theta)$
 537 is the directional wave breaking saturation spectra:

$$B(f) = \int_0^{2\pi} B(f, \theta) d\theta = E(f) \left(\frac{2\pi f^5}{2g} \right). \quad (\text{A19})$$

538 The modulation due to long waves is calculated according to Guimarães (2018):

$$M_{LW} = \left[1 + p_3 \sqrt{\text{cmss}(E(f))} \cos^2(\theta - \hat{\theta}) \right]^{p_4} \quad (\text{A20})$$

539 where $p_3 = 400$ and $p_4 = 3/2$ are also best-fit constants found by Romero (2019). The
 540 cumulative mean square slope (cmss) is defined as:

$$\text{cmss} = \int_0^\infty E(f) \left(\frac{(2\pi)^4 f^4}{g^2} \right) df. \quad (\text{A21})$$

541 and

$$\hat{\theta} = \tan \left(\frac{\int E(f, \theta) \sin(\theta) df d\theta}{\int E(f, \theta) \cos(\theta) df d\theta} \right) \quad (\text{A22})$$

542 The modulation due to the wind is computed as:

$$M_W = \frac{\left(1 + p_5 \max \left(1, \frac{f}{f_0} \right) \right)}{\left(1 + p_5 \right)} \quad (\text{A23})$$

543 with

$$f_0 = p_6 \frac{1}{u_*} \frac{g}{2\pi} \quad (\text{A24})$$

544 where $p_5 = 0.9$ is a constant related to the DIA algorithm and $p_6 = 3/28$ is yet another
 545 constant. Finally, the conversion from $\Lambda(f)$ to $\Lambda(c)$ is done using the relation $\Lambda(c)dc =$
 546 $\Lambda(f)df$ and the linear dispersion relation (see Romero's (2019) Eqs. 17-23 for details).

547 **Acknowledgments**

548 This work benefited from France Energies Marines and State financing managed
 549 by the National Research Agency under the Investments for the Future program bear-
 550 ing the reference numbers ANR-10-IED-0006-14 and ANR-10-IEED-0006-26 for the projects
 551 DiME and CARAVELE. The authors' thank Peter Sutherland and Jim Thompson for
 552 kindly sharing their data.

553 **Data Availability**

554 All data used in this publication has been previously published by Banner et al.
 555 (2000), Sutherland and Melville (2013), Schwendeman et al. (2014).

556 **References**

- 557 Alsina, J. M., & Baldock, T. E. (2007). Improved representation of breaking wave
 558 energy dissipation in parametric wave transformation models. *Coastal Engi-
 559 neering*, *54*, 765–769. doi: 10.1016/j.coastaleng.2007.05.005
- 560 Ardag, D., & Resio, D. T. (2020). A new approach for modeling dissipation due to
 561 breaking in wind wave spectra. *Journal of Physical Oceanography*, *50*(2), 439–
 562 454.
- 563 Ardhuin, F., Rogers, E., Babanin, A. V., Filipot, J. F., Magne, R., Roland, A., ...
 564 Collard, F. (2010). Semiempirical dissipation source functions for ocean waves.
 565 Part I: Definition, calibration, and validation. *Journal of Physical Oceanogra-
 566 phy*, *40*(9), 1917–1941. doi: 10.1175/2010JPO4324.1
- 567 Banner, M. L., Babanin, A. V., & Young, I. R. (2000). Breaking Probability for
 568 Dominant Waves on the Sea Surface. *Journal of Physical Oceanography*,
 569 *30*(12), 3145–3160. doi: 10.1175/1520-0485(2000)030<3145:BPFDWO>2.0.CO;
 570 2
- 571 Banner, M. L., Gemmrich, J. R., & Farmer, D. M. (2002). Multiscale measurements
 572 of ocean wave breaking probability. *Journal of Physical Oceanography*, *32*(12),
 573 3364–3375. doi: 10.1175/1520-0485(2002)032<3364:MMOOWB>2.0.CO;2
- 574 Banner, M. L., & Morison, R. P. (2010). Refined source terms in wind wave
 575 models with explicit wave breaking prediction. Part I: Model framework
 576 and validation against field data. *Ocean Modelling*, *33*(1-2), 177–189. Re-
 577 trieved from <http://dx.doi.org/10.1016/j.ocemod.2010.01.002> doi:

578 10.1016/j.ocemod.2010.01.002

579 Banner, M. L., & Tian, X. (1998). On the determination of the onset of breaking
580 for modulating surface gravity water waves. *Journal of Fluid Mechanics*, 367,
581 107–137.

582 Banner, M. L., Zappa, C. J., & Gemmrich, J. R. (2014). A note on the Phillips spec-
583 tral framework for ocean whitecaps. *Journal of Physical Oceanography*, 44(7),
584 1727–1734. doi: 10.1175/JPO-D-13-0126.1

585 Barthelemy, X., Banner, M. L., Peirson, W. L., Fedele, F., Allis, M., & Dias, F.
586 (2018). On a unified breaking onset threshold for gravity waves in deep and
587 intermediate depth water. *Journal of Fluid Mechanics*, 841, 463–488. doi:
588 10.1017/jfm.2018.93

589 Battjes, J. A., & Janssen, J. (1978). Energy loss and set-up due to breaking of ran-
590 dom waves. *Coastal Engineering*, 32(1), 569–587.

591 Chawla, A., & Kirby, J. T. (2002). Monochromatic and random wave breaking at
592 blocking points. *Journal of Geophysical Research: Oceans*, 107(C7), 4–1.

593 Cokelet, E. D. (1977). Steep Gravity Waves in Water of Arbitrary Uniform Depth.
594 *Philosophical Transactions of the Royal Society A: Mathematical, Physical*
595 *and Engineering Sciences*, 286(1335), 183–230. Retrieved from [http://](http://rsta.royalsocietypublishing.org/cgi/doi/10.1098/rsta.1977.0113)
596 rsta.royalsocietypublishing.org/cgi/doi/10.1098/rsta.1977.0113
597 doi: 10.1098/rsta.1977.0113

598 Dean, R. G. (1965). Stream Function Representation of Nonlinear Ocean Waves.
599 *Journal of Geophysical Research*, 70(18), 4561–4572.

600 Derakhti, M., Kirby, J. T., Banner, M. L., Grilli, S. T., & Thomson, J. (2020).
601 A unified breaking onset criterion for surface gravity water waves in arbi-
602 trary depth. *Journal of Geophysical Research: Oceans*(2013), 1–28. doi:
603 10.1029/2019jc015886

604 Donelan, M., Longuet-Higgins, M., & Turner, J. (1972). Periodicity in whitecaps.
605 *Nature*, 239(5373), 449–451.

606 Duncan, J. H. (1981). An Experimental Investigation of Breaking Waves Pro-
607 duced by a Towed Hydrofoil. *Proceedings of the Royal Society A: Mathe-*
608 *matical, Physical and Engineering Sciences*, 377(1770), 331–348. Retrieved
609 from [http://rspa.royalsocietypublishing.org/cgi/doi/10.1098/](http://rspa.royalsocietypublishing.org/cgi/doi/10.1098/rspa.1981.0127)
610 [rspa.1981.0127](http://rspa.royalsocietypublishing.org/cgi/doi/10.1098/rspa.1981.0127) doi: 10.1098/rspa.1981.0127

- 611 Eldeberky, Y., & Battjes, J. A. (1996). Spectral modeling of wave breaking: Ap-
 612 plication to Boussinesq equations. *Journal of Geophysical Research*, *101*, 1253–
 613 1264.
- 614 Filipot, J. F., & Ardhuin, F. (2012). A unified spectral parameterization for wave
 615 breaking: From the deep ocean to the surf zone. *Journal of Geophysical Re-
 616 search: Oceans*, *117*(4), 1–19. doi: 10.1029/2011JC007784
- 617 Filipot, J. F., Ardhuin, F., & Babanin, A. V. (2010). A unified deep-to-shallow
 618 water wave-breaking probability parameterization. *Journal of Geophysical Re-
 619 search: Oceans*, *115*(4), 1–15. doi: 10.1029/2009JC005448
- 620 Filipot, J.-F., Guimaraes, P., Leckler, F., Hortsmann, J., Carrasco, R., Leroy, E.,
 621 ... Le Dantec, N. (2019). La Jument lighthouse: a real-scale laboratory for
 622 the study of giant waves and their loading on marine structures. *Philosophical
 623 Transactions of the Royal Society A: Mathematical, Physical and Engineering
 624 Sciences*, *377*(2155), 20190008. doi: 10.1098/rsta.2019.0008
- 625 Gemmrich, J., Zappa, C. J., Banner, M. L., & Morison, R. P. (2013). Wave break-
 626 ing in developing and mature seas. *Journal of Geophysical Research: Oceans*,
 627 *118*(9), 4542–4552. doi: 10.1002/jgrc.20334
- 628 Guimarães, P. V. (2018). *Sea surface and energy dissipation* (Unpublished doctoral
 629 dissertation). Université de Bretagne Loire.
- 630 Holland, K. T., Holman, R. A., Lippmann, T. C., Stanley, J., Member, A., & Plant,
 631 N. (1997). Practical Use of Video Imagery in Nearshore Oceanographic Field
 632 Studies. *IEEE Journal of Oceanic Engineering*, *22*(1), 81–92.
- 633 Holthuijsen, L., & Herbers, T. (1986). Statistics of breaking waves observed as
 634 whitecaps in the open sea. *Journal of Physical Oceanography*, *16*(2), 290–297.
- 635 Hwang, P. A., Wang, D. W., Walsh, E. J., Krabill, W. B., & Swift, R. N. (2000).
 636 Airborne Measurements of the Wavenumber Spectra of Ocean Surface Waves.
 637 Part II: Directional Distribution. *Journal of Physical Oceanography*, *30*(11),
 638 2768–2787. doi: 10.1175/1520-0485(2001)031<2768:amotws>2.0.co;2
- 639 Janssen, T. T., & Battjes, J. A. (2007). A note on wave energy dissipation over
 640 steep beaches. *Coastal Engineering*, *54*(9), 711–716. doi: 10.1016/j.coastaleng
 641 .2007.05.006
- 642 Kjeldsen, S. P., Vinje, T. P., Myrhaug, D. P., & Brdvig, P. P. (1980). Kinematics of
 643 deep water breaking waves. In *Offshore technology conference*.

- 644 Kleiss, J. M., & Melville, W. K. (2011). The analysis of sea surface imagery for
 645 whitecap kinematics. *Journal of Atmospheric and Oceanic Technology*, *28*(2),
 646 219–243. doi: 10.1175/2010JTECHO744.1
- 647 Kudryavtsev, V., Chapron, B., & Makin, V. (2014). Impact of wind waves on the
 648 air-sea fluxes: A coupled model. *Journal of Geophysical Research: Oceans*,
 649 *119*(2), 1217–1236.
- 650 Le Méhauté, B. (1962). On non-saturated breakers and the wave run-up. *Proceed-*
 651 *ings of the 8th International Conference on Coastal Engineering*(Figure 1),
 652 77–92. Retrieved from [http://journals.tdl.org/icce/index.php/icce/](http://journals.tdl.org/icce/index.php/icce/article/viewArticle/2255)
 653 [article/viewArticle/2255](http://journals.tdl.org/icce/index.php/icce/article/viewArticle/2255)
- 654 Longuet-Higgins, M. S. (1957). The Statistical Analysis of a Random, Moving Sur-
 655 face. *Philosophical Transactions of the Royal Society A: Mathematical, Physi-*
 656 *cal and Engineering Sciences*, *249*(966), 321–387. doi: 10.1098/rsta.1957.0002
- 657 Melville, W. K., & Matusov, P. (2002). Distribution of breaking waves at the ocean
 658 surface. *Nature*, *417*(6884), 58–63. doi: 10.1038/417058a
- 659 Miche, A. (1944). Mouvements ondulatoires de la mer en profondeur croissante ou
 660 décroissante. Première partie. Mouvements ondulatoires périodiques et cylin-
 661 driques en profondeur constante. *Annales des Ponts et Chaussées, Tome 114*,
 662 42–78.
- 663 Perlin, M., Choi, W., & Tian, Z. (2013). Breaking Waves in Deep and Intermedi-
 664 ate Waters. *Annual Review of Fluid Mechanics*, *45*(1), 115–145. doi: 10.1146/
 665 annurev-fluid-011212-140721
- 666 Phillips, O. M. (1985). Spectral and statistical properties of the equilibrium range in
 667 wind-generated gravity waves. *Journal of Fluid Mechanics*, *156*, 505–531. doi:
 668 10.1017/S0022112085002221
- 669 Reul, N., & Chapron, B. (2003). A model of sea-foam thickness distribution for pas-
 670 sive microwave remote sensing applications. *Journal of Geophysical Research*
 671 *C: Oceans*, *108*(10), 19–1. doi: 10.1029/2003jc001887
- 672 Rice, S. O. (1944). Mathematical Analysis of Random Noise. *The Bell System Tech-*
 673 *nical Journal*, *23*(3), 282 – 332. doi: [https://doi.org/10.1002/j.1538-7305.1944](https://doi.org/10.1002/j.1538-7305.1944.tb00874.x)
 674 [.tb00874.x](https://doi.org/10.1002/j.1538-7305.1944.tb00874.x)
- 675 Romero, L. (2019). Distribution of Surface Wave Breaking Fronts. *Geophysical Re-*
 676 *search Letters*, *46*(17-18), 10463–10474. doi: 10.1029/2019GL083408

- 677 Saket, A., Peirson, W. L., Banner, M. L., Barthelemy, X., & Allis, M. J. (2017). On
 678 the threshold for wave breaking of two-dimensional deep water wave groups in
 679 the absence and presence of wind. *Journal of Fluid Mechanics*, *811*, 642.
- 680 Schwendeman, M., Thomson, J., & Gemmrich, J. R. (2014). Wave breaking dissipa-
 681 tion in a Young Wind Sea. *Journal of Physical Oceanography*, *44*(1), 104–127.
 682 doi: 10.1175/JPO-D-12-0237.1
- 683 Sutherland, P., & Melville, W. K. (2013). Field measurements and scaling of ocean
 684 surface wave-breaking statistics. *Geophysical Research Letters*, *40*(12), 3074–
 685 3079. doi: 10.1002/grl.50584
- 686 Thomson, J. (2012). Wave breaking dissipation observed with "swift" drifters. *Jour-
 687 nal of Atmospheric and Oceanic Technology*, *29*(12), 1866–1882. doi: 10.1175/
 688 JTECH-D-12-00018.1
- 689 Thomson, J., & Jessup, A. T. (2009). A fourier-based method for the distribution of
 690 breaking crests from video observations. *Journal of Atmospheric and Oceanic
 691 Technology*, *26*(8), 1663–1671. doi: 10.1175/2009JTECHO622.1
- 692 Thornton, E. B., & Guza, R. T. (1983). Transformation of Wave Height Distribu-
 693 tion. *Journal of Geophysical Research*, *88*(C10), 5925–5938.
- 694 Varing, A., Filipot, J.-f., Grilli, S., Duarte, R., Roeber, V., & Yates, M. (2020).
 695 A new kinematic breaking onset criterion for spilling and plunging breaking
 696 waves in shallow water. *Coastal Engineering*, 1–24.
- 697 Zieger, S., Babanin, A. V., Erick Rogers, W., & Young, I. R. (2015). Observation-
 698 based source terms in the third-generation wave model WAVEWATCH. *Ocean
 699 Modelling*, *96*(Vic), 2–25. Retrieved from [http://dx.doi.org/10.1016/
 700 j.ocemod.2015.07.014](http://dx.doi.org/10.1016/j.ocemod.2015.07.014) doi: 10.1016/j.ocemod.2015.07.014